DEVELOPMENTAL DYNAMICS 219:182–191 (2000)

Modeling the Interplay of Generic and Genetic Mechanisms in Cleavage, Blastulation, and Gastrulation

DIRK DRASDO[1] AND GABOR FORGACS[2,3]*
[1]*Institute for Medical Informatics, Statistics, and Epidemiology, University of Leipzig, Leipzig, Germany*
[2]*Department of Physics and Biology, Clarkson University, Potsdam, New York*
[3]*Department of Physics and Biology, University of Missouri, Columbia, Missouri*

ABSTRACT **Early development of multicellular organisms is marked by a rapid initial increase in their cell numbers, accompanied by spectacular morphogenetic processes leading to the gradual formation of organs of characteristic shapes. During morphogenesis, through differentiation under strict genetic control, cells become more and more specialized. Morphogenesis also requires coordinated cell movement and elaborate interactions between cells, governed by fundamental physical or generic principles. As a consequence, early development must rely on an intricate interplay of generic and genetic mechanisms. We present the results of computer simulations of the first nontrivial morphogenetic transformations in the life of multicellular organisms: initial cleavages, blastula formation, and gastrulation. The same model, which is based on the physical properties of individual cells and their interactions, describes all these processes. The genetic code determines the values of the model parameters. The model accurately reproduces the major steps of early development. It predicts that physical constraints strongly influence the timing of gastrulation. Gastrulation must occur prior to the appearance of dynamical instability, which would destabilize and eventually derail normal development. Within our model, to avoid the instability, we suddenly change the values of some of the model parameters. We interpret this change as a consequence of specific gene activity. After changing the physical characteristics of some cells, normal development resumes, and gastrulation proceeds.** © 2000 Wiley-Liss, Inc.

Key words: blastula; gastrulation; physical mechanisms; computer

INTRODUCTION

After fertilization, many multicellular organisms go through a sequence of cleavages leading to a layer of rapidly dividing cells enclosing a hollow spheroidal blastula (Gilbert, 1997; Wolpert, 1998). Subsequently, the layer folds, and gastrulation takes place, during which the animal builds its digestive system and feeding apparatus. Blastula formation and gastrulation are the earliest manifestations of morphogenesis, the set of pattern-forming mechanisms that create complex biological forms out of simpler structures. A fundamental question in developmental biology is what drives morphogenesis? What determines the morphology of the developing organism? According to one view, forms and patterns result from the unique program encoded in the DNA. Another view holds that the determining factors of morphogenesis are epigenetic, intrinsic self-organizing properties of tissues, analogous to other viscoelastic materials. Neither of these extreme views can adequately describe developmental phenomena (Gurdon, 1992), and the genetic and generic-physical properties must interplay (Newman and Comper, 1990). The embryo produces the "building material" (e.g., proteins) for its development from the available nutrients, according to the rules embodied in its genetic code. Then diffusion, spreading, differential adhesion, chemotaxis, and so on transport these building materials to specific regions of the developing organism. The transport of matter obeys the laws of physics. The mechanical or chemical changes that may take place during transport (changes in concentration, cell shape, adhesiveness and cohesiveness, etc.) are signals (Dolmetsh et al., 1997) that often influence the production of the building material itself, that is, gene activity.

Early morphogenesis, in particular epithelial folding (Etteshon, 1985) during gastrulation, has been studied extensively in various organisms, and a number of models have been proposed. In the more biological models, like the one of Leptin and Grunewald (1990) for *Drosophila* gastrulation, the correct execution of patterning requires the coordinated activity of specific maternal and zygotic genes. The more physical models (Odell et al., 1980, 1981; Davidson et al., 1995; 1999 for sea urchin gastrulation) rely on generic processes, the mechanical properties of individual cells (Hiramoto, 1968, 1969; Hochmuth et al., 1993) or tissues (Drasdo et al., 1995; Foty et al., 1996; Forgacs et al., 1998), and

Grant sponsor: Deutsche Forschungsgemeinschaft; Grant number: LO 342/4-3; Grant sponsor: National Science Foundation; Grant number: IBN-9710010.
*Correspondence to: Gabor Forgacs, Department of Physics and Biology, Clarkson University, Potsdam, NY 13699–5820.
E-mail: forgacs@clarkson.edu
Received 20 January 2000; Accepted 30 May 2000

contain adjustable parameters. Since the relationship between the model parameters and the specific molecular building blocks of the organism are not known, despite great efforts, the precise mechanism of epithelial folding remains elusive.

Our primary motivation is the realization that understanding the full course of development requires understanding the interplay between genetic and generic processes. We introduce a dynamical model of early morphogenesis based on specific properties of cells and their interactions known to play a fundamental role in folding. Based on the model we perform extensive computer simulations of blastula formation and gastrulation. We show how properties like cell shape or strength of cell adhesion, when under strict genetic control, naturally constrain morphological phenomena. The distinguishing feature of our approach is that we are able to follow developmental pattern formation from the initial cleavages through blastula formation up to gastrulation using essentially the same model, only modifying its parameters. The specific values of these parameters for a given organism at a given time reflect biological specificity.

Our objective is not to "build an animal," and to reproduce minute details of blastula formation and gastrulation using physics and mathematics. Despite spectacular progress in molecular biology, biochemistry, and biophysics, quantitative information on developmental processes is scarce. A model reproducing every aspect of early morphogenesis cannot be realistic, even for a particular animal. We hope to illustrate for a specific developmental process how to relate morphogenetic changes to measurable physical properties and to suggest how to tie these properties to the molecular alphabet of cells and tissues.

RESULTS

Model for Early Morphogenesis

The first nontrivial cellular structure that appears in the developing multicellular organism is the blastula. It may be fully symmetric (radial holoblastic cleavage, e.g., in the sea cucumber Synapta digita) or possess lower symmetry, as in some worms (spiral holoblastic cleavage), tunicates (bilateral holoblastic cleavage), or mammals (rotational holoblastic cleavage). The degree of synchronization of cell division and the orientation of cell division planes determine the symmetry of the blastula. In animals that show radial holoblastic cleavage, synchronization may either be perfect (as in the sea cucumber) or, in later stages, show differences between the vegetal and animal pole, as in the sea urchin (Gilbert, 1997).

Two theories try to explain the formation and expansion of the blastocoele. Dan (1960) hypothesized that the motive force of this expansion is the blastocoele itself. As the blastomeres secrete proteins into the blastocoele, the blastocoele fluid becomes syrupy. This blastocoele sap absorbs large quantities of water by osmosis, thereby swelling and putting pressure on the blastomeres to expand outward. Wolpert and Mercer (1963) have proposed that this effect does not need pressure from the blastocoele. They emphasize the role of differential adhesion between the cells and to the hyaline layer enclosing them. These authors point out that as long as cells remain strongly attached to the hyaline layer, they do not have an alternative but to expand. This expansion creates the blastula, rather than the other way around.

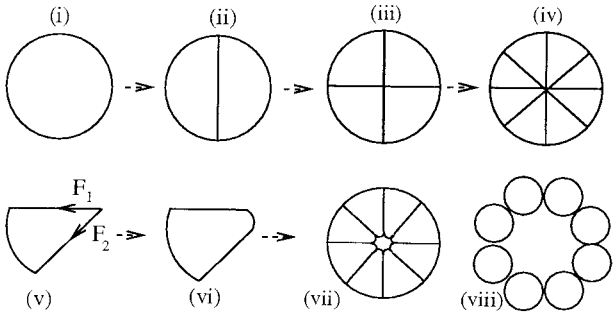

Fig. 1. Schematic sequence of cell divisions (shown in two dimensions) for holoblastic cleavage. (i)–(iv) illustrate an idealized situation with the daughter cells occupying the original volume of the zygote. (v) shows a particular daughter cell from the eight-cell stage. Its membrane, at the periphery and at the center of the cell configuration shown in (iv), has extremely sharp turns. The edges have very high bending energy and, as a consequence, experience a force $\vec{F}_1 + \vec{F}_2$ opposing the curve, as indicated in (v) (forces are shown only for the center). Depending on the bending rigidity (the extent to which a material resists bending) of the membrane, the rounding of each cell in (iv) results in a cell configuration similar to (vii) (small bending rigidity) or (viii) (large bending rigidity). The requirement that a change in cell shape leave the total cell mass, or cell volume unchanged leads to a net displacement of cell mass away from the center.

In the present work we propose a mechanism for blastula formation and gastrulation in the case of perfect holoblastic cleavage. The proposed mechanism is based on the properties of individual cells and their direct interactions. Below we summarize the major features of our model and its assumptions.

1. During formation of a hollow spherical blastula and, subsequently, of the gastrula, cell division proceeds at constant embryo mass. The total number of cells grows exponentially to several thousands (Gilbert, 1997).
2. Cells remain cuboid during cleavage. Therefore, strong bends or kinks in the material of their membrane are energetically disfavored. Thus, we assume that large changes in the local geometry (i.e., curvature) of the membrane generate a restoring force, which tends to flatten the variation in geometry. As Fig. 1 illustrates, such an assumption requires that during cleavage the cell mass shifts outward, away from the center of the embryo.
3. Cells bind to an extracellular hyaline layer. Hence the mechanical properties of the cell layer and the extracellular layer determine those of the blastula and the gastrula (Davidson et al., 1999). In reality,

cells also attach to the basal and apical lamina. Since their effect on the mechanical properties is considerably weaker (Gilbert, 1997; Davidson et al., 1995) we neglect them.

4. Cells in the early embryo are polar and, as a consequence of the inhomogeneous distribution of their adhesion molecules, form cell-cell contacts in special regions of their membrane, resulting in preferred cell configurations (Wolpert, 1998) that we believe correspond to local minima in the (free) energy. Deviations from preferred cell shapes and configurations increase the energy. In our model, the energy of a cell configuration contains the following contributions.
   (i) An interaction energy of neighboring cells. Embryonic cells in contact form adhesive bonds. With decreasing distance between the centers of the cells (e.g., upon compression) their contact area and, with it, the number of adhesive contacts increase, resulting in an attractive interaction. On the other hand, if cells are spheroid in isolation, a large contact area between them significantly stresses their membranes or, equivalently, costs steric entropy (Helfrich, 1978). Furthermore, it is reasonable to assume that under physiological conditions cells have a small compressibility. The loss of entropy and limited compressibility give rise to a repulsive interaction.

   The manifestation of local physical interactions (i.e., between individual cells) at larger scale (i.e., blastula) is quite insensitive to the detailed shape of the corresponding interaction energy (Odell et al., 1981; Drasdo et al., 1995; Drasdo, 1996). We therefore model the combination of the repulsive and attractive energy contributions by the interaction energy shown in Fig. 2. (Mathematical details on the interaction energy are collected in the Appendix.)

   The physical interactions responsible for these competing energy contributions have a characteristic range δ, determined by the deformability and the glycocalix of the cell, the properties of the hyaline layer, and the nature of cell adhesion molecules. Such interactions are typically short range. Since cells interact directly only with their closest neighbors, δ in Fig. 2 is larger than the width of the glycocalix but does not exceed the radius of an uncompressed cell. The elastic properties of the cell layer and the surrounding hyaline layer determine the shape of the interaction energy within δ by the parameter ϵ, as shown in Fig. 2.
   (ii) Polar cells have characteristic apical and basal surfaces. They form contacts with their neighbors along the lateral part of their membranes and often form two-dimensional, single-cell layers or epithelial sheets. The preferred geometry of the layer and the shape of the cells within the layer depend on the location of cell adhesion molecules, as shown schematically in Fig. 3a. Analogous to polymer membranes, the preferred shape of the sheet at the position of the i-th cell, has a local "spontaneous curvature" c_i (Lipowsky, 1991). (The curvature of a curve at point i is $1/r_i$, where r_i, the local radius of curvature, is the radius of the circle that matches the curve at that point; the curvature of a straight line is everywhere zero. In the local minimum energy state $1/r_i = c_i$.) Any bending of the sheet distorts the membranes and consequently the cytoskeleton of the cells making up the sheet, resulting in a deviation of the curvature of the sheet from the spontaneous curvature ($1/r_i \neq c_i$), and consequently in the increase of energy associated with the membrane's bending (Helfrich, 1978; Lipowsky, 1991) and the cytoskeleton distortion. The energy of bending (away from the preferred shape) depends on the material of the sheet: the more rigid the sheet, the more difficult it is to bend. This resistance to bending defines the effective bending rigidity κ of the epithelial sheet (Lipowsky, 1991). Whereas the preferred shape of the individual cell i (characterized by the angle β_0 in Fig. 3a) exclusively determines the spontaneous curvature c_i, once it is part of a tissue layer, the actual curvature of the sheet (r_2 in Fig. 3c) depends also on the positions of the cells' neighbors. If cell i changes its shape actively (for example, owing to differentiation that may alter its cytoskeleton or the distribution of cell adhe-

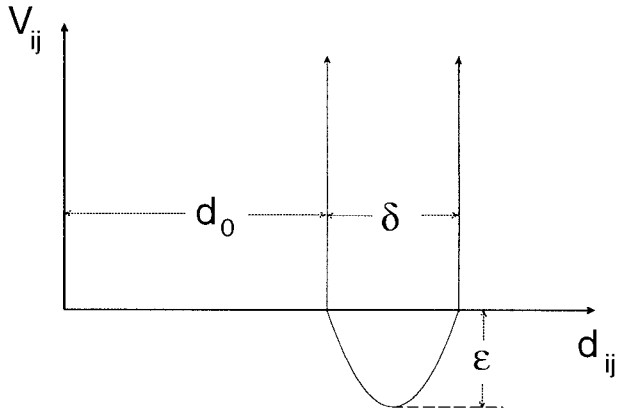

Fig. 2.. The interaction energy V_{ij} in the contact region between two neighboring cells i and j as a function of the distance d_{ij} between the centers of the cells. The shape of V_{ij} reflects the limited compressibility of the cells (d_{ij} cannot be smaller than a minimal distance d_0) and incorporates the entropic contributions of their membranes. Furthermore, it contains direct cell-cell adhesion and the elastic contribution of an attempt to separate cells. The value of V_{ij} at $d_o + \delta$ ($V_{ij} = \infty$) forces cells to remain in contact during blastula formation and gastrulation. δ includes the range over which a cell can be stretched or compressed in a certain direction as well as the interaction range of cell adhesion molecules. Hence, δ is the range of interaction between neighboring cells.

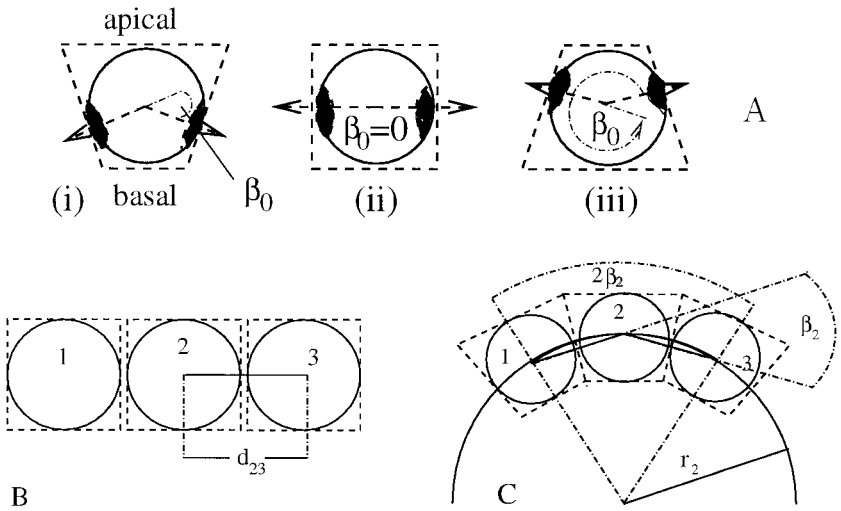

Fig. 3. **A:** Preferred individual cell shapes depending on the location of adhesion molecules (black areas). In this two-dimensional representation, the angle β_0 uniquely determines the preferred shape of the cell and therefore the local spontaneous curvature, c_s. Circles with the associated angles demarcate the simplified shape we use to represent cells in the simulations. The optimal configuration of a sheet containing only cells with preferred shapes (i) or (iii) is a closed surface with the basal lamina oriented either toward the interior [(i), $\beta_0 < \pi$] or toward the exterior [(iii), $\beta_0 > \pi$]. **B:** Preferred cell shape (ii) ($\beta_0 = 0$) results in an optimal configuration with an open, planar cell sheet and equal distance between the centers of (identical) cells. **C:** Deviation from the optimal configuration shown in panel B. For cell type (ii) any bend (characterized by finite local radius of curvature r and deviation angle β) increases the bending energy. (Here the radius of curvature and the deviation angle are shown only for cell 2.) Note that for cell type (i) the illustrated configuration is optimal if $\beta_j = \beta_0$, where j denotes any cell in the sheet.

sion molecules along its membrane), it affects the shape of neighboring cells as well, by changing the local curvature of the tissue sheet in the vicinity of cell i. If none of the neighboring cells resists the change in shape of cell i, cell i exclusively determines the local radius of curvature r_i by $r_i = 1/c_i$; bending of the sheet does not cost energy. In the idealized situation, when all cells in a given arrangement are identical (of the same type, at the same point in the cell cycle, etc.), the spontaneous curvature is the same for all of them (i.e. $c_i = c$ independent of i). The explicit mathematical form of the bending energy, in terms of c_i, κ and r_i, used in this work is given in the Appendix.

5. Active cell movement characterizes early morphogenesis. This movement, which leads to the appearance of new forms, on one hand must satisfy the constraints imposed by the activity of maternal and zygotic genes and on the other hand should proceed according to the governing physical mechanisms, which exert forces on the cells. These forces depend on the explicit form of the interaction energy and bending energy discussed earlier as well as many other factors and should eventually lead to configurations with minimal mechanical stresses (at least temporarily). In order to incorporate additional factors, we assume that during cleavage extracellular components provide a friction-like resistance to the displacements and orientational changes of the cells within the developing tissue sheet. The stronger the friction, the slower the cells move. Our model incorporates friction and additional biological and chemical processes, like metabolism, intra- and extracellular transport, movements of the cytoplasm, and the reorganization of the cytoskeleton by imposing an additional stochastic force on the cells.
6. The mobility, geometric environment, and the interaction of a cell with its neighbors affect the observed cell cycle time. The cycle time also depends on the cell's intrinsic properties, which we incorporate by introducing the intrinsic cell cycle time τ. We interpret τ as a quantity that may change through purely chemical means (e.g., by growth and inhibition factors). For an isolated cell not affected by physical interactions with neighboring cells, τ is the average cell cycle time. If excluded volume interactions are present, the observed cell cycle time τ_R is typically larger than the intrinsic cycle time, that is, $\tau_R \geq \tau$.

We simulate friction-limited stochastic dynamics, driven by physical interactions due to mechanical forces, as described earlier, using the Monte Carlo method (Metropolis et al., 1953; for an application to growth in tissues, see Drasdo, 1996). Such simulations in three dimensions are extremely time consuming. Our simulations in this work are two-dimensional, equivalent to considering only spherically (e.g., sea urchin) or axially (e.g., sea cucumber) symmetric embryos (the issue of dimensionality is discussed in Drasdo, 2000). Thus, all the figures showing cell configurations can be interpreted as two-dimensional projections of three-dimensional structures. (We cannot exclude with certainty that fundamentally new phenomena do not occur in three-dimensional simulations, which will be performed in the future.) The section on experimental procedures gives details on the simulation algorithms.

We have introduced several parameters, such as the characteristic strength (ϵ) and range (δ) of cellular interactions, as well as spontaneous curvature (c), bending rigidity (κ), and intrinsic cell cycle time (τ). In the course of development, the rules embodied in the genetic code determine and control the change in the values of these parameters. We assume that most of the time this change is not too rapid. If it were, these parameters would have no meaning and any effort to interpret aspects of morphogenesis in terms of physical models would be futile.

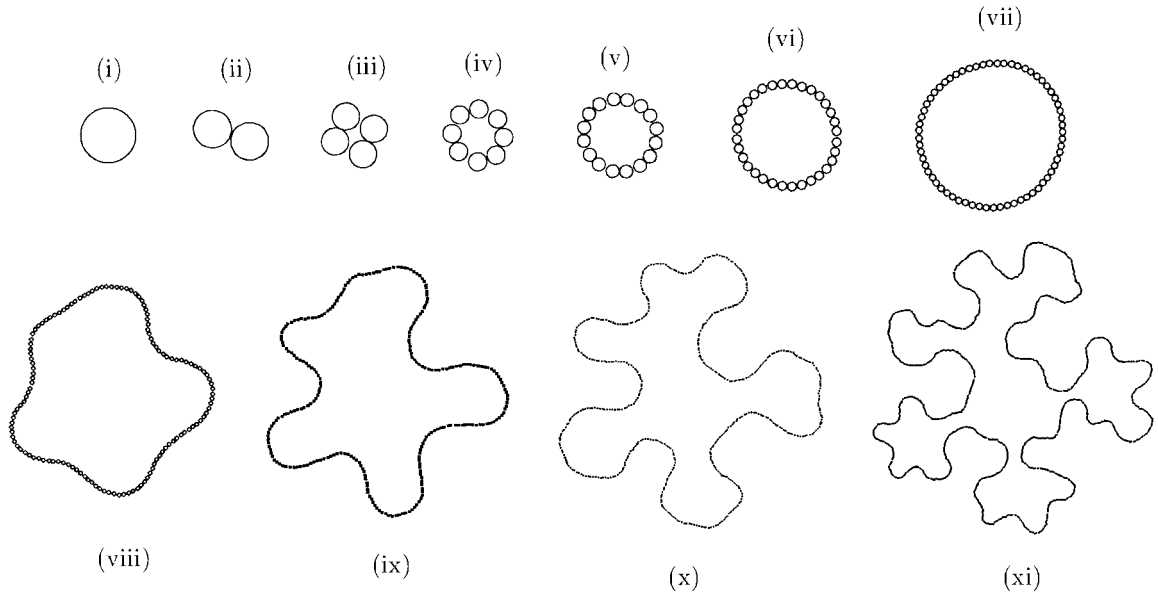

Fig. 4. The evolution of the cellular pattern in the computer simulation for $\epsilon(0) = 7 \times 10^6$ kcal/mol and $\kappa(0) = 5 \times 10^4$ kcal m/mol. As explained in the Appendix, the magnitudes of these parameters vary with the size of the cells, i.e. with the number of cell divisions, m. The above values refer to the zygote ($m = 0$). For the chosen values of ϵ and κ configurations (i)–(vii) correspond to normal development. A dynamical instability sets in after the 64-cell stage (vii), which in a spherical embryo would correspond to about 2,000 cells. (Owing to the uncertainties in the experimental values of $\epsilon(0)$ and $\kappa(0)$, such an instability would not necessarily occur at the 2,000-cell stage. Furthermore, shear energy (which may occur in three dimensions) or an osmotic pressure may alter the onset of the instability. With further growth of the cell population, the folding of the blastula becomes more pronounced, as seen in patterns (viii)–(xi).

Blastula Formation

We start our simulations with a single cell and terminate them either when the number of cells reaches $N = 1{,}024$ or when a particular cell acquires more than two neighbors. Figure 4 shows the result of a typical simulation. The number of cells grows exponentially, and after a series of cell divisions a hollow spherical blastula forms. With further divisions spherical symmetry disappears; the blastula becomes unstable and folds. Within our model this instability is generic and shows up over a wide range of parameter values. Figure 5 summarizes the sensitivity of blastula formation to changes in cell elasticity. We vary ϵ, κ, and δ within limits compatible with available experimental information. (The relationship between our model parameters and the experimentally known quantities is discussed in the Appendix.) As the figure reveals, varying the parameters does not affect the appearance of the instability; its occurrence merely shifts in time. (In three dimensions effects nonexistent in two dimensions may further influence the exact timing of the instability.)

The origin of the instability is the following (for a more general discussion, see Drasdo, 2000). The growth and division of cells requires that either individual cells or the entire cell layer be able to migrate. Small stochastic differences in the migration result in undulations in the shape of the sheet, which initially decay owing to the smoothening effect of the bending energy. As cells proliferate, both the number and the extent of these undulations increase. Eventually the bending energy is unable to smooth the sheet and folding takes place. Increasing the value of κ and with it the stabilizing effect of the bending energy postpones folding but does not suppress it. The bending rigidity κ reflects the composite physical properties of both the cell and the hyaline layers and can be modified by various chemicals (Davidson et al., 1999). Davidson et al. (1999) have found that the elastic properties of the hyaline layer determine those of the sea urchin embryo. Thus, it should be possible to study experimentally the correlation between κ and the appearance of the instability, shown in Fig. 5.

We also have varied the intrinsic cell cycle time τ (results not shown; see Drasdo [2000] for the cycle time dependency of the instability). A tenfold variation in τ leads to a crossover from exponential to slower than exponential growth followed again by a geometric instability. Irradiation or growth factors may modify τ; hence we could test this finding experimentally. The results of this section indicate that in the absence of any additional regulatory process, the blastula is bound to fold, derailing normal development.

Gastrulation

The near spherical symmetry of the blastula cannot persist beyond a certain stage of development. The organism must be able to sense the approaching instability and react to it. To avoid folding, with its detri-

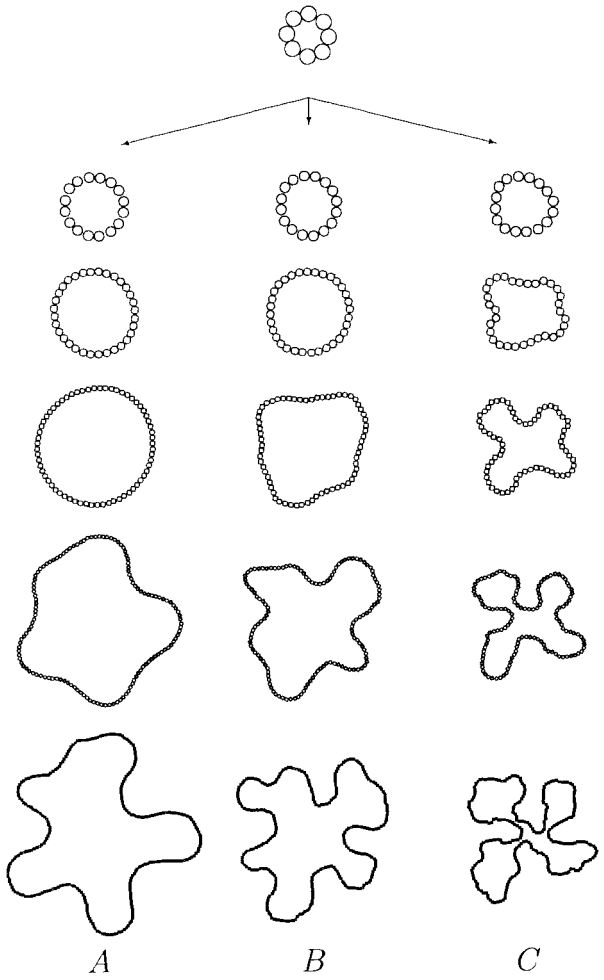

Fig. 5. Sensitivity of blastula formation to changes in cell elasticity. The evolution in column **A** corresponds to Fig. 4. For columns **B** and **C** the values of ϵ and κ are $\epsilon(0) = 2.2 \times 10^6$ kcal/mol and $\kappa(0) = 1.3 \times 10^4$ kcal m/mol (B) and $\epsilon(0) = 1.5 \times 10^6$ kcal/mol and $\kappa(0) = 3 \times 10^3$ kcal m/mol (C), respectively. Up to the eight-cell stage the patterns evolve identically. For large ϵ and κ the dynamical instability develops later.

mental consequences on normal development, genetic mechanisms must lead to differentiation and, with it, to changes in physical parameters. In the sea urchin, near the vegetal pole of the blastula a distinct group of cells appears—the primary mesenchymal cells. Concomitant with this differentiation, the blastula flattens, cell division slows down and eventually stops, and gastrulation starts. Gastrulation involves the motion of a large number of cells to invaginate the blastula around the vegetal pole. In our model, invagination requires a drastic change in the bending energy, accomplished by assuming that differentiation of cells near the vegetal pole modifies their spontaneous curvature, which until now was zero. (In two dimensions the circle is the configuration with minimum energy for all choices of spontaneous curvature, as long as all cells have the same spontaneous curvature [Drasdo, 2000]).

For sea urchin gastrulation (Odell et al., 1980, 1981; Davidson et al., 1995, 1999) we know the values of most of the model parameters within certain limits (for a comprehensive list, see Davidson et al., 1995), or they can be determined (see Appendix). Sea urchin gastrulation starts at around the 1,000-cell stage, corresponding to about 50 cells along the perimeter in the two-dimensional circular cut of the blastula. For realistic values of the model parameters, the folding instability develops after the 64-cell stage (Fig. 4). To avoid this instability, we assign cells at the 64-cell stage in the "contractile region" (with the size of 11 cells in Figs. 6 and 7) nonzero spontaneous curvature c, which, within our model, corresponds to differentiation. Simulations leading to Figs. 6 and 7 used a gradient in c. Cells at the edge of the contractile region have the smallest absolute value of c, which increases toward the center. If c is positive, the model leads to an exogastrula. At this point we do not know how to relate c to specific genes or molecular parameters. However, the figures show that its distribution can describe quite accurately the real gastrula (Gilbert, 1997).

Invaginating cells actively change their shape (hence the term *contractile region*). In our model the shape deformation of cells drives gastrulation (and blastulation). In Figs. 6 and 7 we represent cells by circles corresponding to epithelial cells of various shapes, as explained in Figs. 3 and 8.

DISCUSSION

Early morphogenesis in multicellular organisms leads to spectacular forms that develop from simple cellular structures. According to the widely held view, such pattern-forming processes are driven and controlled by morphogens, specific chemicals. Chemicals, however, do not define the rules for cellular motion accompanying developmental changes. Physical interactions and underlying laws do. It is these physical laws that restrict the possible forms and shapes that cellular patterns may adopt.

Our dynamical model describes early morphogenesis, starting with fertilization and ending with primary invagination in gastrulation, based on realistic physical interactions between individual cells. Genetic mechanisms specify the values of the parameters characterizing these physical interactions. In our model differentiation modifies these values. In this way, instead of constructing another physical model to describe post-blastula development, we are able to use the original model with slightly changed parameters. Normal development then may continue, and the model leads to primary invagination signaling the onset of gastrulation.

Davidson et al. (1995) studied five different models of primary invagination, which considered the embryo to be an elastic body and invagination to be driven by various parts of this body (e.g., by the microfilament network in the apical constriction model or by the contraction of cells in the vegetal plate in the apico-

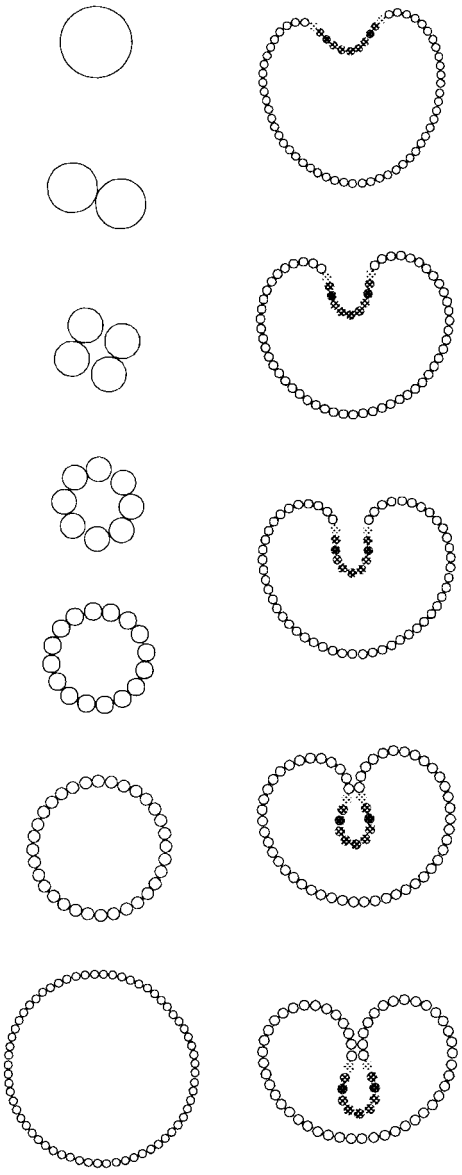

Fig. 6. Gastrulation for $\epsilon = 7 \times 10^6$ kcal/mol and $\kappa = 5 \times 10^4$ kcal m/mol. At the 64-cell stage (last figure in the left column) differentiation (i) suppresses further cell divisions (thus ϵ and κ do not change their values) and (ii) changes the cytoskeleton of the shaded 11 cells in such a way that the spontaneous curvature locally becomes negative. From the leftmost cell 1 to the rightmost cell 11, the spontaneous curvatures follow the pattern $c_1, c_2, c_3, c_4, c_5, c_6, c_5, c_4, c_3, c_2, c_1$, with $c_i = \Delta \times i$ (i.e., cells 1 and 11, 2 and 10, etc., have pairwise the same spontaneous curvatures). Here, $\Delta = -2$. Note that involution occurs simultaneously in the whole invaginating region, as pointed out by Kam et al. (1991).

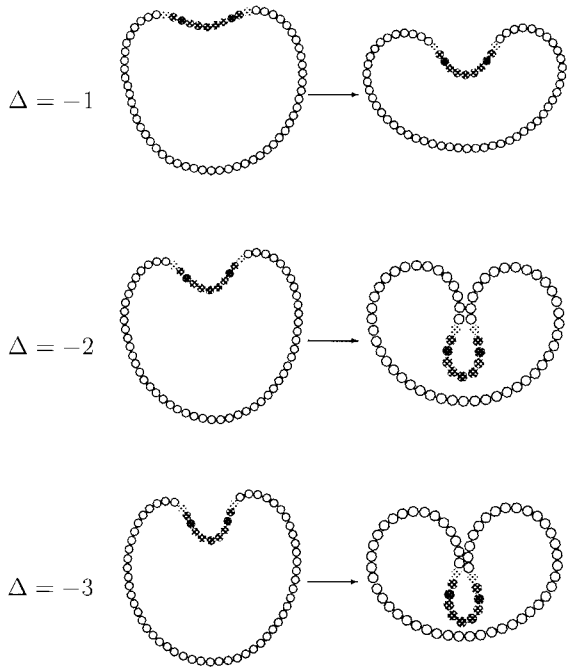

Fig. 7. Cell configurations at the onset of gastrulation (left column) and at the end of gastrulation (right column) for various values of Δ. For $\Delta \sim -2$ the proposed mechanism allows the archenteron to invaginate about two-thirds of its full length, which corresponds to the physiological situation.

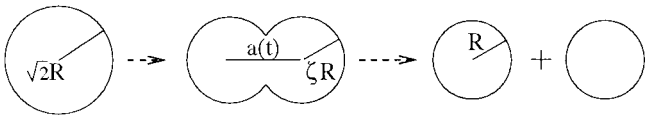

Fig. 8. Cell division in the simulation. The cell deforms by decreasing its instantaneous radius (in its maximally compressed state) $R(t) = \zeta(t)R$ ($\zeta(t) < 1$) from R (at $t = 0$) $\rightarrow R/\sqrt{2}$ (at $t = \tau_R$) in small steps ξ, where ξ is a uniformly distributed random number in the interval $0 \leq \xi \leq \xi^{max}$ with $\xi^{max} \ll R$. The quantity $\zeta(t)$ contains information on the cumulative effect of these small steps. Accordingly, the axis $a(t)$ increases to keep the total area of the cell constant during one division cycle. The dumbbell shape ensures constant area. On a time scale larger than the cell cycle time, this choice of the cell division algorithm should not influence the final results (for a more detailed discussion on this point, see Drasdo, 1996). R denotes the radius of a cell in its maximally compressed state, which corresponds to the minimal distance d_0 (Fig. 2) between the centers of neighboring cells (immediately after division) or the centers of the nearest circles of neighboring dumbbells (during cleavage). The true linear extent of a cell depends on both R and δ (for details see the Appendix).

basal contraction model). Recently, the same authors have measured the composite elastic modulus of the cellular and extracellular matrix layers of Strongylocentrotust purpuratus embryos at the mesenchyme blastula stage, to restrict the proposed physical mechanisms for gastrulation (Davidson et al., 1999).

Our model of early development can describe several morphogenetic transformations (e.g., blastula formation and primary invagination) and incorporates both physical processes and cell division. The model predicts correlations among the onset of instability in the shape of the blastula, the rate of mitosis, and the model parameters, which are experimentally accessible. These correlations can be studied experimentally (along the lines of Davidson et al. [1999]). Our results suggest that the shape of the blastula may represent a checkpoint for gastrulation. The dynamical instability also may serve to distinguish between Dan's hypothe-

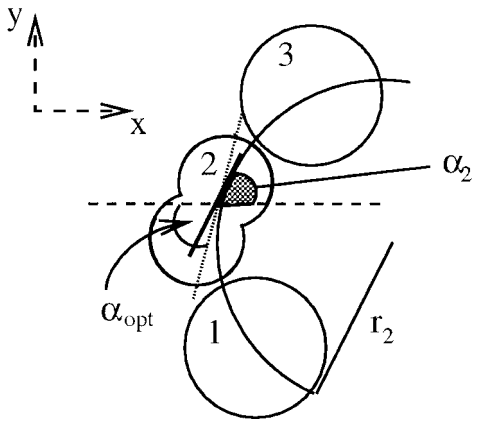

Fig. 9. Determination of the cell division plane in the simulation. The angle α_2 (shaded area) between its axis $a(t)$ (Fig. 8) and the x-axis determines the instantaneous orientation of cell 2. In our two-dimensional model this orientation is optimal if $a(t)$ is tangential (denoted by the dotted line) to the local radius of curvature r_2, constructed according to Fig. 3c. The optimal orientation of $a(t)$ defines α_{opt}, the optimal value of α_2. We construct the angle α_{opt} to ensure that the daughter cells of a cell that has just divided again fit into the tissue sheet.

sis (Dan, 1960) and ours, because if osmotic pressure is the major driving force for the blastocoele expansion, we would not expect an instability to occur.

We hope that with this work we have resolved in part the problem posed by Bissell and Barcellos-Hoff (1987): "The concept that shape per se regulates function is difficult to translate into mechanism: what is needed is a translation of 'shape' into an alphabet of molecules and discrete steps."

EXPERIMENTAL PROCEDURES

Monte Carlo Simulation

We used the following algorithms in our simulations.

A. Cell division is implemented by the rule illustrated in Fig. 8. After each division a chosen cell (see later discussion) deforms in small steps. We assume its shape immediately after each division to be a circle whose radius depends on the number of divisions it has experienced. We reject steps that lead to overlap between adjacent cells (*excluded volume effect*) and again attempt to deform the chosen cell. Since the total cell mass remains constant during cleavage, the deformation must preserve the area of the cell. Therefore R_m, the cell radius after a cell has performed the m-th division decreases with m as $R_m \sim 1/\sqrt{2^m}$. R denotes the radius of a maximally compressed cell (for the true cell size, see the Appendix). Accordingly, we choose $\delta_m \sim 1/\sqrt{2^m}$, which also ensures that the interaction range δ does not exceed the radius of the cell.

B. Each cell reorients toward an optimal orientation guided by the rotational energy for dumbbell-shaped cells (see Fig. 9). This rule recognizes the well-defined orientation of cleavage planes and the fact that cells are able to orient their mitotic spindles according to the positions of their neighbors (White and Borisy, 1983). The specific form of the rotational energy is given in the Appendix.

C. The simulation chooses a cell randomly and modifies its state by shape deformation (see caption to Fig. 8), displacement, or rotation. The magnitudes of these changes are chosen randomly from a uniform distribution. If such a modification increases energy, the cell returns to its original position with a probability $P = 1 - \exp(-\Delta V/F_T)$; otherwise it stays in its new position. Here, $\Delta V = V' - V$, where V and V' are the total energies of the entire cell assembly, respectively, before and after the change in the state of the randomly chosen single cell. The energy of a cell configuration contains the total interaction energy, total bending energy, and total rotational energy. For cells that perform a pure random walk, $\Delta V = 0$ and all changes in the state of a cell are accepted. F_T is a reference energy (Beysens et al., 1998), analogous to the thermal energy k_BT in fluids or gases (T: physical temperature, k_B: Boltzmann constant). We assume F_T to be of the order of the metabolic energy of a single cell. Because we do not know its value during blastula formation, it remains a model parameter. (Beysens et al. [1998] estimated $F_T \approx 10^5$ kcal/mol for chicken embryonic cells.)

D. In many embryos early cell divisions are fully (or partially) synchronized: all the cells (or groups of cells) in the developing organism divide at the same time and (within a group) are of the same size. Synchronization may be driven by a chemical whose concentration shows a wavelike pattern with a maximum in mitosis (M-phase-promoting factor; Alberts et al., [1994]). To simulate fully synchronized cell division, we perform cytokinesis, the last step in the cell cycle, only if all cells of a given arrangement have arrived at this step. Hence cells that already have completed mitosis "wait" for cytokinesis until all other cells in the configuration are also ready for this step. Accordingly, for fully synchronized cell division, the total number of cells doubles in each cycle, and immediately after cell division is completed each cell has the same size. Hence, the number of cells after the zygote has performed m cleavages is $N = 2^m$.

Computer

Most simulations employed Pentium 450 processors. Depending on the choice of parameters, a run took between 1 and 7 days of CPU time of a single processor.

Units

Our simulations use numbers. To relate these numbers to physical quantities requires the introduction of physical units, that is, a time scale, a length scale, and an energy scale. As a length scale we have chosen the diameter of the zygote (50 μm), and as a time scale we

chose the cell cycle time τ. For the simulations presented in this work, $\tau = 1$ hr. The reference energy F_T discussed earlier provides the energy scale, $F_T = 10^5$ kcal/mol. All times, lengths, and energies become multiples of the chosen scales.

ACKNOWLEDGMENT

This work was supported by the Deutsche Forschungsgemeinschaft under grant LO 342/4-3 (to D.D.) and by the National Science Foundation under grant IBN-9710010 (to G.F.). We acknowledge the hospitality of the Max-Planck-Institute for Colloid and Interfacial Science in Golm and the Collegium Budapest, where part of the work was carried out. We thank an anonymous referee for useful comments.

REFERENCES

Alberts B, Bray D, Lewis J, Raff M, Roberts K, Watson JD. 1994. Molecular biology of the cell. New York: Garland.

Beysens DA, Forgacs G, Glazier JA. 1998. Networks of droplets induced by coalescence: application to cell sorting. In: Beysens DA, Forgacs G, editors. Dynamical networks in physics and biology. New York: Springer. p 161–169.

Bissell MJ, Barcellos-Hoff MH. 1987. Influence of ECM on gene expression. J Cell Sci 8(suppl):327–343.

Dan K. 1960. Cytoembryology of echinoderms and amphibia. Int Rev Cytol 9:321–367.

Davidson LA, Koehl MAR, Keller R, Oster GF. 1995. How do sea urchins invaginate? Using biomechanics to distinguish between mechanisms of primary invagination. Development 121:2005–2018.

Davidson LA, Oster GF, Keller R, Koehl MAR. 1999. Measurements of mechanical properties of the blastula wall reveal which hypothesized mechanisms of primary invagination are plausible in the sea urchin Strogylocentrotus purpuratus. Dev Biol 209:221–238.

Dolmetsh RE, Lewis RS, Goodnow CC, Healy JI. 1997. Differential activation of transcription factors induced by Ca^{2+} response amplitude and duration. Nature 386:855–858.

Drasdo D. 1996. Different growth regimes found in a Monte Carlo model of growing tissue cell populations. In: Schweitzer F, editor. Self-organization of complex structures: from individual to collective dynamics. London: Gordon and Breach. p 281–292.

Drasdo D. Buckling instabilities in one-layered growing tissues. 2000. Phys Rev Lett 84:4424–4427.

Drasdo D, Kree R, McCaskill JS. 1995. Monte Carlo approach to tissue-cell populations. Phys Rev E 52:6635–6657.

Etteshon CA. 1985. Mechanisms of epithelial invagination. Q Rev Biol 60:289–307.

Forgacs G, Foty RA, Shafrir Y, Steinberg MS. 1998. Viscoelastic properties of living tissues: a quantitative study. Biophys J 74: 2227–2234.

Foty RA, Pfleger CM, Forgacs G, Steinberg MS. 1996. Surface tensions of embryonic tissues predict their envelopment behavior. Development 122:1611–1620.

Gilbert SF. 1997. Developmental biology. Sunderland, MA: Sinauer Associates.

Gurdon JB. 1992. The generation of diversity and pattern in animal development. Cell 68:185–199.

Helfrich W. 1978. Steric interactions of fluid membranes in multilayer systems. Z Naturforsch A 33:305–315.

Hiramoto Y. 1968. Observation and measurements of sea urchin eggs with a centrifuge microscope. J Cell Physiol 69:219–230.

Hiramoto Y. 1969. Mechanical properties of the protoplasm of the sea urchin egg. Exp Cell Res 56:201–208.

Hochmuth RH, Ting-Beall HP, Beaty BB, Needham D, Tran-San-Tay R. 1993. Viscosity of passive human neutrophils undergoing small deformations. Biophys J 69:1596–1601.

Kam Z, Minden J, Agard D, Sedat JW, Leptin M. 1991. *Drosophila* gastrulation: analysis of cell shape changes in living embryos by three-dimensional fluorescence microscopy. Development 112:365–370.

Leptin M, Grunewald B. 1990. Cell shape changes during gastrulation in *Drosophila.* Development 110:73–84.

Lipowsky R. 1991. The conformation of membranes. Nature 349:475–481.

Metropolis N, Rosenbluth AW, Rosenbluth MN, Teller AH, Teller E. 1953. Equation of state calculations by fast computing machines. J Chem Phys 21:1087–1092.

Newman SA, Comper W. 1990. Generic physical mechanisms of morphogenesis and pattern formation. Development 110:1–18.

Odell GM, Oster G, Burnside B, Alberch P. 1980. A mechanical model for epithelial morphogenesis. J Math Biol 9:291–295.

Odell GM, Oster G, Alberch P, Burnside B. 1981. The mechanical basis of morphogenesis. Dev Biol 85:446–462.

White JG, Borisy GG. 1983. On the mechanism of cytokinesis in animal cells. J Theor Biol 101:289–316.

Wolpert L. 1998. Principles of development. Oxford: Oxford University Press.

Wolpert L, Mercer EH. 1963. An electron microscope study of the development of the blastula of the sea urchin embryo and its radial polarity. Exp Cell Res 30:280–300.

APPENDIX

This Appendix gives some details of the mathematics used in the simulations.

We start the simulations with a single cell, the zygote, whose linear dimensions initially are $d_x = d_y = d_z = 50$ μ, corresponding to a sea urchin egg immediately after fertilization. Because our simulations are two-dimensional, cells divide only in the x-y plane, and their extension perpendicular to this plane stays constant (initial $d_z = 50$ μ). Thus, a "real" cell in the simulations, immediately after cell division has the shape shown in Fig. 10. During cleavage, the cell elon-

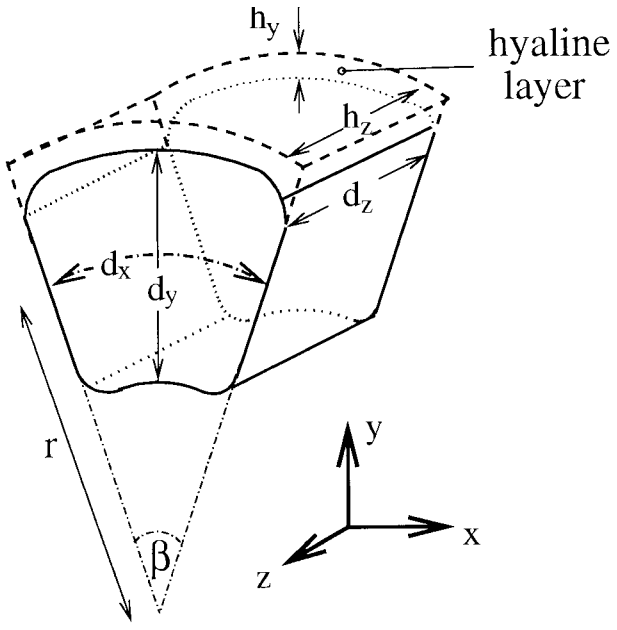

Fig. 10. Sketch of a cell with the hyaline layer. The hyaline layer has a thickness $h_y = 1$ μm. The linear dimensions of the cell in the x, y, and z directions are, respectively, d_x, d_y, and d_z. Figure 3 shows the projection of the cell onto the x-y plane and defines the quantities r and β.

gates in the x-direction and shortens in the y-direction (Fig. 8).

Blastula formation conserves total embryo mass, so the area of a cell in the x-y plane decreases by a factor of 2 with each cell division. Therefore, immediately after the m-th division $d_x(m) = d_y(m) = d_x(0)/\sqrt{2^m}$.

The total energy is

$$V = V^{NN} + V^B + V^R, \tag{1}$$

where V^{NN} is the total nearest-neighbor interaction energy, V^B the total bending energy, and V^R the total rotational energy.

Once contacts have formed, owing to their elastic properties, cells resist compression or stretching, causing an elastic contribution to V^{NN}. A further elastic contribution, which we incorporate into V^{NN}, arises from the attachment of the cells to the hyaline layer. The nearest neighbor energy for the composite system becomes $V^{NN} = \Sigma_{ij} V_{ij}^{NN}$, where V_{ij} is the interaction energy of nearest neighbor cells i and j:

$$V_{ij}^{NN} = \begin{cases} \epsilon\left(\left[1 - \dfrac{2d_{ij} - 2\{R_i + R_j\}}{\delta}\right]^2 - 1\right) \\ \qquad \text{if} \quad R_i + R_j \le d_{ij} \le R_i + R_j + \delta \\ \infty \quad \text{otherwise} \end{cases} \tag{2}$$

Here $d_{ij}(t)$ denotes the distance between the centers of the nearest circles of the neighboring dumbbells i and j. (Consider a figure similar to Fig. 9, where dumbbells replace circles 1 and 3.) Each dumbbell consists of two circles of instantaneous radius $R(t)$ and an axis of length $a(t)$ (Fig. 8). A circular cell is a dumbbell with axis length $a = 0$. As mentioned, R denotes the appropriate radius under maximal compression. δ is the range over which a cell can change its size under tension or compression.

V_{ij}^{NN} diverges for $d_{ij} = R_i + R_j$ and $d_{ij} = R_i + R_j + \delta$ and has a minimum at $d_{ij} = R_i + R_j + \delta/2$. d_{ij} relates to the size of a cell i as follows: the distance between the nearest circles of dumbbells i and j is $d_{ij} - R_i - R_j$; hence, the size of cell i parallel to its axis (taken to be the x-axis in Fig. 10) with its left neighbor $i - 1$ and its right neighbor $i + 1$ is

$$d_x = R_i + \frac{d_{i,i-1} - R_i - R_{i-1}}{2} + a_i + R_i + \frac{d_{i,i+1} - R_i - R_{i+1}}{2}. \tag{3}$$

For a cell i that is neither compressed nor stretched, $\dfrac{d_{i,i-1} - R_i - R_{i-1}}{2} = \dfrac{d_{i,i+1} - R_i - R_{i+1}}{2} = \dfrac{\delta}{4}$; hence, its size parallel to its axis is $2R_i + a_i + \delta/2$. Thus, the true size of a circular cell ($a_i = 0$) depends both on R_i, its radius in its maximally compressed state, and the range of cell-cell interactions.

The magnitude of δ decreases with each cell division, similarly to d_x and d_y. Thus, after the m-th division $\delta(m) = \delta(0)/\sqrt{2^m}$, and we choose $\delta(0) = 0.1 d_x(0)$ as an estimate for the range over which a cell can be stretched or compressed in a certain direction (G. Yagil, personal communication). The expression for d_x above, together with the requirement of constant mass, determines the height d_y.

The bending energy is

$$V^B = \frac{\kappa}{2} \sum_i \left(\frac{1}{r_i} - c_i\right)^2 r_i \beta_i, \tag{4}$$

where c_i is the spontaneous curvature, r_i the local radius of curvature at the position of cell i, and $2\beta_i$ the angle between cells $i - 1$ and $i + 1$ (see Fig. 3c). The bending rigidity κ, similar to ϵ in Eq. 2, contains the contribution of both the cell and hyaline layers.

If the stress to which cells are exposed during blastula formation is sufficiently small, we may treat them as linear springs (Odell et al., 1981) and express ϵ and κ in Eqs. 2 and 3 in terms of the material and geometric properties of the cell and the hyaline layers (as shown in Fig. 10). Their dependence on the geometry requires recalculation of κ and ϵ after each cell division, so they both depend on the number of cell divisions m. The appropriate material constants are the Young's moduli of the cell and hyaline layers listed by Davidson et al. (1995) for the sea urchin. Using these values and the appropriate geometric parameters, we arrive at $\epsilon(0) = 7 \times 10^6$ kcal/mol and $\kappa(0) = 5 \times 10^4$ kcal m/mol for the zygote at $m = 0$.

In order to ensure the correct orientation of the cell division plane, we assume that cells are able to orient their mitotic spindle to maintain a one-cell-thick structure. Our model accomplishes this by introducing the orientational rotational energy $V^R = \Sigma_i V_i^R$, with

$$V_i^R = \gamma(\alpha_i - \alpha_i^{\text{opt}})^2 \tag{5}$$

Fig. 9 defines α_i and α_i^{opt}. We set $\gamma \gg 1$ to avoid excessive deviations of α_i from α_i^{opt}.

Finally, the strength of friction that cells experience in the course of their displacements and orientational changes is expressed in terms of a friction constant. Its magnitude η (related to the reference energy F_T and the cell diffusion coefficient D as $\eta = F_T/D$) is taken from the work of Beysens et al. (1998), $\eta(0) \approx 11$ kg/s.